EXPERIMENTAL STUDY OF HIGH–POWER RADIATION PROPAGATION ALONG AN ATMOSPHERIC PATH

V.A. Banakh, V.M. Sazanovich, and R.Sh. Tsvyk

Institute of Atmospheric Optics,
Siberian Branch of the Russian Academy of Sciences, Tomsk
Received September 21, 1994

Some results of an integrated experimental study of the influence of thermal nonlinearity on the distortions of laser radiation propagating along an atmospheric path are presented. Such effects accompanying propagation of high–power radiation as attenuation, defocusing, and beam shift are analyzed depending on the propagation conditions. Some results of the experiments on measuring optical parameters of the medium within the propagation channel done with visible sounding beams are presented also. A nonlinear thermal lens formed at the beginning of propagation, in the case of stable transverse wind, is shown to determine the distortion of high–power laser radiation at the end of the propagation path.

Propagation of high–power laser radiation (HPLR) through the atmosphere is accompanied by nonlinear effects being determined by the absorbed energy, duration of radiation, parameters of laser beam, etc. Thermal blooming arising as a result of air heating due to absorption of laser energy is one of the most widespread and low–threshold nonlinear effects.[1,3]

When pulse–periodic radiation is used, the acoustic waves propagating perpendicular to the direction of the HPLR propagation play an essential role in forming of the propagation channel. If the pulse duration τ_p is much less than the time of sound travel across the channel, $\tau_p < a/V_s$, and the pulse repetition frequency is much less than V_s/a, an influence of the acoustic waves on the HPLR can be neglected. At the same time, the acoustic waves can essentially affect parameters of sounding beams propagating through the HPLR channel.

In real atmosphere the absorption of radiation along the propagation path causes heating of the channel and, hence, the air refractive index decreases and beam defocusing appears. Wind, in its turn, blows out heat from the channel, thus changing the intensity distribution and the beam cross section shape, and shifts the beam energy center towards the wind.[3] These simplest aberrations make the greatest contribution to the beam distortions but can be effectively corrected using adaptive optics[4] by introducing predistortions into the initial field allowing for the refractive index distribution along the induced channel.

At present there are no accurate analytical and numerical methods to solve the problem on the HPLR propagation accounting for all the variety of distorting factors. That is why reference (sounding) beams passing through the propagation channel are used to obtain information on the structure of the refractive index field to provide beam control. However, experiments with sounding beams sometimes are difficult for performance because of constructive peculiarities in the optics forming a high–power laser beam.

Experiments in the atmosphere as well as under laboratory conditions and comparison of obtained data with theoretical calculations are very important for verification of the model of HPLR interaction with the atmosphere and for prediction of beam distortions. In this paper we present a summary of our investigations of HPLR distortions observed in real atmosphere and we also make an attempt here to use known similarity parameters describing nonlinearities in light propagation when interpreting our experimental results.

Laser radiation with the wavelength $\lambda = 10.6$ μm was used in the experiment. The laser operated in the pulse–periodic regime. The atmospheric path passed over an open place 3–4 m above a smooth underlying surface. Because of the heat transfer in the area of interaction between radiation and the atmosphere and in connection with the specific experimental conditions the path was divided into two segments. The initial segment of the path between the source and forming optics was characterized by high energy density and heat transfer due to convection. Such sections (stagnation areas[2]) cause a considerable beam defocusing and shift due to the medium heating. The atmospheric segment of the path from the forming optics to the target was characterized by a large extent, focusing of radiation to the target plane, and heat outflow from the interaction area due to transverse wind. A ratio of the length of the initial segment of the path to the length of the atmospheric one was 1:50.

The measurements were carried out with the following equipment:

– the power meter for measuring total power and pulse duration at the output of HPLR source;

– the array of thermocouples with time response of 0.1 s for measuring the energy distribution over the reception plane;

– the equipment for measuring meteorological parameters and atmospheric transmission along the propagation path;

– the equipment complex for sounding the propagation channel.

1. The loss of radiation energy along a path is one of the most important characteristics of atmospheric influence on radiation. For radiation with the wavelength $\lambda = 10.6$ μm attenuation is mainly due to absorption by carbon dioxide and water vapor molecules and scattering by aerosol. Experimentally the transfer ratio K_t was determined from the ratio of energy measured by the

0235-6880/95/03 241-06 $02.00

thermocouple array at the path end to the energy at the output of the laser. The measured transfer ratios were compared with the calculated atmospheric transmission T_{calc} which was determined by the formula[5]:

$$T_{calc} = \exp \{- [\alpha_{ab} + A\ \alpha_{aer}\ (0.63)]\ L\} \qquad (1)$$

where $\alpha_{ab} = \alpha_{H_2O} + \alpha_{CO_2}$ is the absorption coefficient for the water vapor and carbon dioxide calculated from the measured values of temperature, humidity, pressure, and mean concentration of the carbon dioxide (0.033%) using the procedure proposed in Ref. 6; α_{aer} is the aerosol extinction coefficient, it was determined from the measured data for the atmospheric transmission at the wavelength 0.63 μm and scaled to the wavelength of the used source[5]

$$\alpha_{aer}\ (10.6) = A\ \alpha_{aer}\ (0.63)\ ,$$

L is the distance which the beam passed trough the medium.

For the conditions of measurements corresponding to the stable spring–fall and summer hazes A equals 0.1. Several runs of measurements were carried out in the experiment. Every next run was performed after some improvements in the equipment undertaken to rise the transfer ratio K_t. The results of two runs are presented in Fig. 1, where the experimental points for the first run are depicted allowing for absorption and scattering, and for the second run the results allow for absorption only. Straight lines illustrate the processing of the experimental data by the least–squares technique: *1* and *2* are for the first and second run accounting for the absorption and scattering, and *3* is for the second run accounting for absorption only. Equations of the straight lines are as follow

$$K_t\,1 = -0.07 + 0.58\ T_{calc}\ , \quad R1 = 0.56\ ,$$

$$K_t\,2 = 0.09 + 0.53\ T_{calc}\ , \quad R2 = 0.54\ ,$$

$$K_t\,3 = -\ 0.105 + 0.767\ T_{calc}\ , \quad R3 = 0.72\ .$$

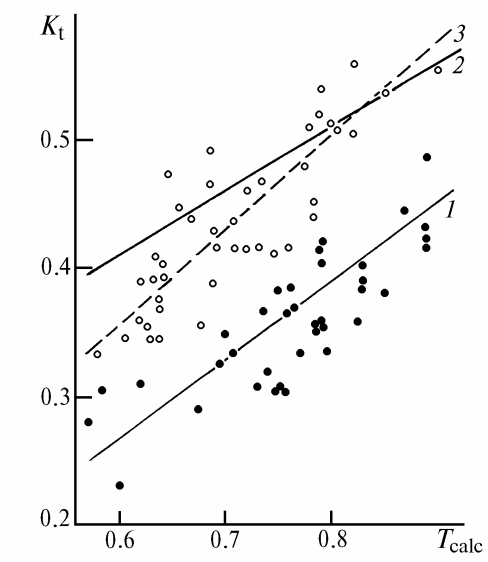

FIG. 1. The atmospheric transmission T_{calc} calculated from the meteorological parameters as compared to the transfer ratio K_t measured.

As is seen from Fig. 1, $K_t < 1$ for $T_{calc} = 1$. This means that in addition to the losses due to absorption and scattering accounted another energy losses occur at the beam optical path, such as losses at the optical system mirrors, possible but ignored losses in the atmosphere due to the nonlinear scattering by the heat induced halo around heated aerosol particles and acoustic waves of density, incoherent part of the radiation diverging at the large angles and being measured at the output of generator but not reaching the detector. These losses were about 56% in the first run of measurements and 37% in the second one. The increase in the transfer ratio of 19% in the second run is due to higher refraction coefficient of the mirror. A linear relation between the measured transfer ratio and calculated atmospheric transmission confirms applicability of this technique of calculation of the extinction coefficient for high power laser radiation with the wavelength 10.6 μm from the measured meteorological parameters under the conditions of weak turbidity of the atmosphere.

2. To estimate the atmospheric distortions of the HPLR, we use the generalized parameter of nonlinear distortions[3]

$$N_c^0 = -\frac{d\,n}{d\,T}\ \frac{\alpha_{ab}\ L^2\ P_0}{\rho\ C_p\ V_\perp\ \pi\ a^3}\ , \qquad (2)$$

where $\frac{d\,n}{d\,T}$ is the temperature gradient of the atmospheric refractive index, P_0 is the total radiation power, ρ and C_p are the density and heat capacity of a unit gas volume, $V_\perp$ is the wind velocity component perpendicular to the propagation direction, a is the beam radius. The absorption coefficient α_{ab} was calculated from the meteorological parameters.

Since in the experiment no wind could be in the initial segment of the path, the nonlinear distortions parameter N_c was determined there via the velocity of convective motion due to the temperature difference inside the channel and outside it

$$V_{con} = \left(\frac{2\ \alpha_{ab}\ g\ P_0}{\rho\ C_p\ T}\right)^{1/3}\ , \qquad (3)$$

where g is the acceleration due to gravity; T is the medium temperature.

When determining N_c for the atmospheric segment of the path we take into account the losses in the optical channel and those due to HPLR focusing

$$N_c^{at} = N_c(F)\ \frac{2\ F}{F-1}\left[\,1 - \frac{\ln F}{F-1}\,\right], \qquad (4)$$

where $F = a_1/a_f$, a_1 and a_f are the radii of the beam at the output aperture and at its focus.

Since HPLR beam propagated, in our experiments, along a path which could be segmented with respect to the conditions of light propagation we use, when analyzing the exponential data, the nonlinearity parameter which is a sum of such parameters describing the segments of the path $N_c = N_c^{in} + N_c^{at}$. In the experiment the following beam parameters in the target plane were analyzed: the change of maximum energy density, relative change of radius, and shift of the beam center of gravity.

3. Figure 2 presents relative energy density at maximum, in the radiation focusing area, at the path end

$\delta = E_{max}/(kE_0)$ as a function of the N_c parameter, where E_{max} is the energy density at maximum, kE_0 is the output power minus ignored energy loss. Solid line shows the dependence $\delta = 0.22\, N_c^{-0.36}$ calculated by the least–squares method. An analysis of the result shows that in spite of a considerable spread of experimental data and low values of the correlation coefficient ($R = 0.35$) a pronounced tendency of the energy density to decrease when the nonlinearity parameter varies from 0.3 to 2 is observed. One of the causes of such a considerable data spread that exceeds the measurement errors at $N_c < 1$, i.e., when the contributions from the atmospheric path and air stagnation region are comparable, can be due to incorrect account for N_c as an arithmetic sum of the parameters N_c^{in} and N_c^{at}. This means that the contributions from every segment should be weighted.

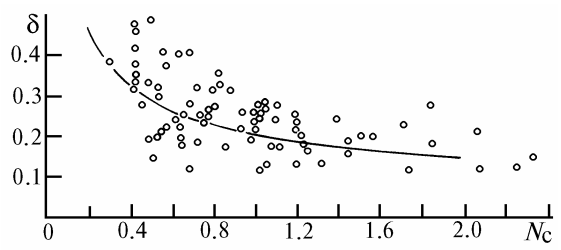

FIG. 2.

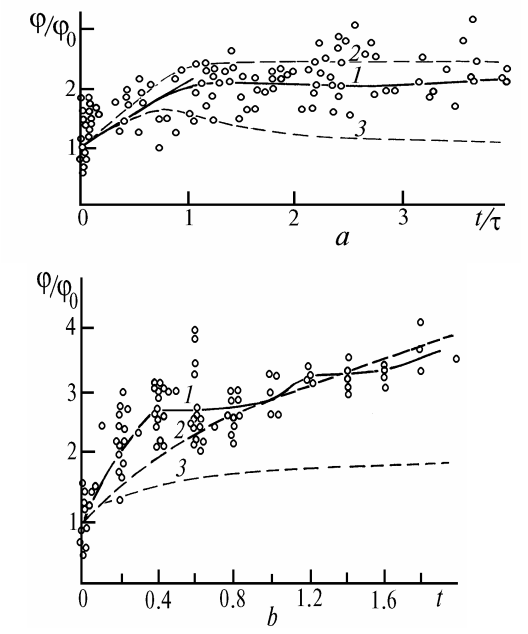

FIG. 3.

4. Analysis of the beam defocusing was carried out using the data on the beam cross section area at the level $0.5E_{max}$ in the measurement plane. The measurement results are divided into two groups depending on the wind velocity at the atmospheric segment of the path. The data from the first group were obtained at the transverse component of the wind velocity $V_\perp > 1$ m/s (Fig. 3 *a*), and the data from the second group at $V_\perp \sim 0$ (Fig. 3 *b*). The beam radius normalized to the radius averaged over the measurements at the end of the path carried out at the moments when the source is switched on is shown on y axis. Estimations have shown that this radius is determined by diffraction on elements of the beam forming optical system and by the turbulence along the atmospheric path. The axis x in Fig. 3 *a* is the time t normalized to the time during which the heat is blown out from the channel $\tau = 2a/V_\perp$. Solid curves *1* in both figures correspond to the mean values of the beam parameters. As is clear from Fig. 3 *a*, at a stable transverse wind the beam size increases practically linearly at $t/\tau < 1$ and reaches stationary defocusing at $t/\tau > 1$. At a weak wind (Fig. 3 *b*), the stationary regime of change of the beam radius was not observed in the experiments when the duration of irradiation was 2–2.5 c. There is the region of rapid increase of the radius at $t = 0$–0.6 s and of its slow increase at $t > 0.6$ s. Beam defocusing is larger than that at the stable wind by a factor of 1.5–2.

Fluctuations of wind velocity and wind direction were not measured in the experiment but these fluctuations are known[7] to affect essentially the radiation defocusing. Dashed curves in Figs. *3a* and *b* are for aberrationless approximation for the source parameters[7] and the following conditions: relative wind velocity fluctuations $\sigma_v/V_\perp = 0$ (curve *2*) and 0.2 (curve *3*), where σ_v is the rms deviation of the transverse wind velocity. The refractive index fluctuations were ignored because the contribution from them to defocusing is small as compared to that from nonlinearity. A comparison of the calculated and experimental data confirms qualitatively the conclusion of the theory describing the influence of characteristic time scales of the wind velocity fluctuations on the time of establishing a stationary regime and on the value of heat defocusing. This coincidence is less satisfactory for the weak or longitudinal wind velocities (Fig. 3 *b*). It is apparently connected with the neglect of inhomogeneity of the propagation path in calculations.

An attempt to find out the dependence of the beam radius on the parameter N_c in a stationary regime has failed. Much more distinct relation is observed between φ and N_c^{in}. Figure 4 presents a comparison of the measured beam radius at $V_\perp > 1$ m/s with that calculated by the formula[2]

$$\varphi_p = 0.8\, N_c\, a\, /\, L, \qquad (5)$$

where the nonlinear distortion parameter was determined in the initial segment of the path. This straight line was calculated by the least–squares method, its equation is

$$j''_{exp} = 5'' + 0.49\, j''_{calc} \qquad (6)$$

with the correlation coefficient $R_{corr} = 0.5$.

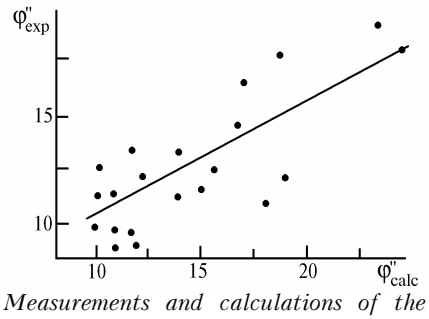

FIG. 4. Measurements and calculations of the angular beam size.

5. The experimental results on shifts of the beam center of gravity were analyzed as a function of wind direction and speed as in the case of the results on defocusing. All measurements are characterized by a large (to 40") initial jump in the position of the beam center of gravity which occurs during the time 0–0.4 s ($t/\tau \le 1$) that corresponds to the time of the medium travel across the beam. In Fig. 5 the position of the beam center of gravity is shown for different moments of time at the cross wind ($V_\perp > 1$ m/s). Shifts mainly occur towards the wind. The shift values reach the radius of the HPLR beam, broadened by the heat nonlinearity, at focus. The most considerable deflections are observed at the longitudinal and weak wind. In the vertical direction (the vertical wind component was not measured) the beam shifts in both directions, and the initial jump during the time of 0.4 s is also observed. No dependence of shifts on the atmospheric conditions has been observed.

Thus, the investigations of the HPLR distortions in the focusing plane did not reveal any certain relation of the beam parameters to conditions of propagation. The inhomogeneity of the propagation path, presence of the stagnation regions where, at a short distance, the nonlinear–distortion parameter N_c reaches the values comparable with N_c at the atmospheric path under stable wind, and correlation of the beam divergence with the values of N_c^{in} have demonstrated the necessity of studying the initial segment in more detail in order to determine its refractive index and the contribution from it into the distortions of the HPLR.

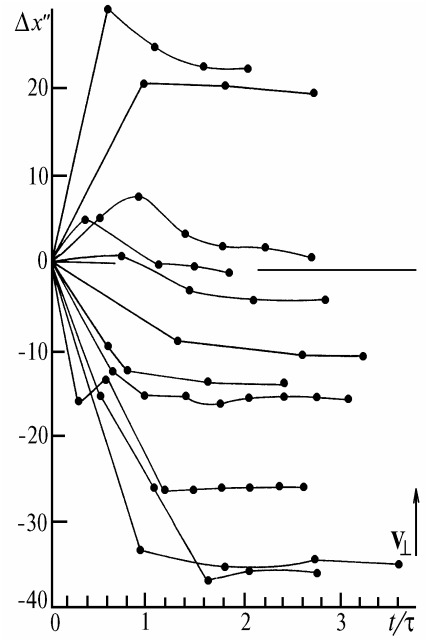

FIG. 5. Displacement of the beam center of gravity (arrow shows the wind direction).

6. The technique of studying the variations of the refractive index within the stagnation segment of the path was in sensing the HPLR channel by a diverging sounding laser beam ($\lambda = 0.63$ μm) propagating at an angle to the HPLR channel, i.e., in measuring shifts of the center of gravity of the sounding beam source image.[8] Such a technique makes it possible to obtain information on the integral change in the refractive index in the region of beams intersection without violating the structure of the main beam.

In our experiments the HPLR channel within the initial segment had a rectangular cross section, its vertical size being twice as large as the horizontal one. The energy density distribution was practically uniform. Because the wind was absent, the heat outflow from the channel occurred due to the molecular heat conduction and natural convection developing owing to the temperature difference inside the channel and outside it. The characteristic time of the convection[3] is $\tau = a/V_{con}$. The values of τ_{con} are within 1 s and the heat conduction time $\tau_\chi = a^2/4\chi > \tau_{con}$ (χ is the air thermal diffusivity) for the absorption coefficient $\alpha_{ab} = (1–3)\ 10^{-6}$ cm^{-1} and for the parameters of the HPLR beam typical for our experiments. Therefore, the effect of thermal diffusion on the process of establishing temperature in the channel can be ignored, and the channel can be considered as a plane plate with the refractive index varying in time.

In accordance with the geometrical optics a ray incident on a plane–parallel plate shifts by the value Δ depending on Δn (Ref. 9)

$$\Delta = d \sin\theta \left[1 - \left(\frac{1 - \sin^2\theta}{n_1^2 - \sin^2\theta}\right)^{1/2}\right], \qquad (7)$$

where d is the cross size of the channel; $n_1 = n - \Delta n$ is the change of the medium refractive index in the channel; θ is the angle of incidence of a sounding beam. In this case the image of the sounding beam source shifts by the value $\rho = \Delta(l/R)$, where l is the distance from the receiving lens to the source image plane; R is the curvature radius of the sounding beam wave front at the receiving lens. In the experiments the position of the center of gravity was measured with a tracking system using a dissector.[10] Before the action the image was set at the center of the dissector photocathode (zero reading). With the beginning of HPLR action the beam image shifted and some time later after the competition of action the image returned to the initial position. The following parameters were determined: the time of the beginning and termination of the action, time and magnitude of the maximum deviation, and time of reaching a steady state. These measurements were carried out simultaneously with the measurements of the energy distribution at the path end. Figure 6 presents the results for several realizations with close values of power of the relative integral change of the refractive index $\Delta n/\Delta n_{max}$ and the changes in relative angular size of the HPLR beam φ/φ_0 in the focusing region when the perpendicular component of the wind velocity within the atmospheric path was $V_\perp > 2$ m/s (φ_0 is the beam angular size at $t = 0$). Figure 6 illustrates a good correlation between the changes in Δn and HPLR beam size at a stable wind. This confirms the above assumption on the influence of the stagnation region on the HPLR distortions. At a weak wind such a correlation was not observed.

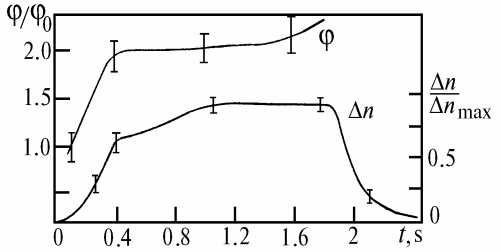

FIG. 6. The angular beam size at the path end compared with Δn in the HPLR channel within the initial segment of the path.

Figure 7 presents the results of comparison of the nonlinearity parameter $N_{c\,exp} = \Delta n\, L^2/a^2$ determined for the maximum value of Δn in the channel and $N_{c\,calc}$ determined from the meteorological data. In this case the convection velocity determined by Eq. (3) was taken as a wind velocity component perpendicular to the beam. It is clear from Fig. 7 that the calculated and measured nonlinearity parameters well correlate within the limits of measurement errors.

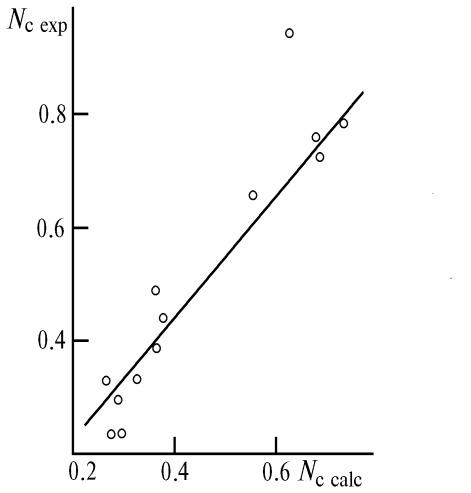

FIG. 7. A comparison of the calculated and measured nonlinear parameters.

7. Shifts of a sounding source image made it possible to determine the change of the refractive index and effective length of a thermal lens. However, a change of spatial spectrum of the refractive index fluctuations can occur in the atmosphere under the HPLR action. This change is due to an additional stochasticity of medium because of heat halos around aerosol particles and effect of acoustic waves of density. To study such changes in the refractive index under the HPLR action, the measurements of intensity fluctuations of sounding radiation of visible range crossing the HPLR channel at the atmospheric path were carried out. The source of sounding radiation was placed near the region of the high–power beam focusing and the receiver was near the output aperture. The cross region was a half of the atmospheric path. The intensity fluctuations were recorded on a magnetic tape and processed with a correlator Kh6–4. The frequency range of recording was 0–10 kHz. Information of the beginning and termination of the HPLR action was recorded simultaneously. The time autocorrelation function of the signal was determined before and during the action by the following formula

$$B(\tau) = \frac{1}{T}\int_0^T I(t)\, I(t-\tau)\, d\, t, \qquad (8)$$

where τ is the time shift; $I(t)$ is the intensity of received signal.

Figure 8 presents the time autocorrelation function in free atmosphere before (curve *2*) and during the HPLR action (curves *4–7*). The numbers of points (time shifts in an arbitrary time scale) are shown on the horizontal axis. As follows from the analysis of the signal shape and correlation functions the contribution to the sounding beam intensity fluctuations from small–scale inhomogeneities of the refractive index or those that rapidly cross the beam increases essentially in the HPLR channel. The second, high–frequency, correlation scale and maximum with a time shift corresponding to the pulse repetition frequency of the HPLR generation appears in all correlation functions under the action. The high–frequency fluctuations power increases with increasing N_c.

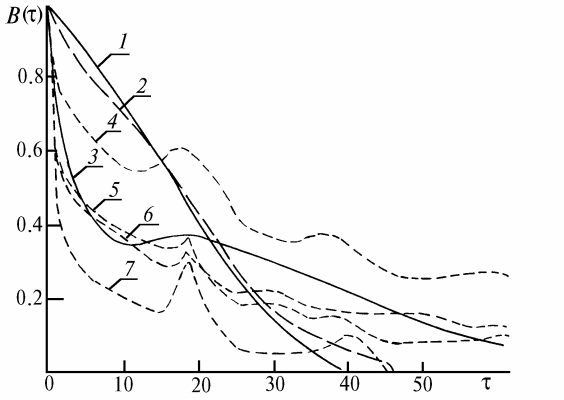

FIG. 8. Time correlation function of a sounding beam intensity: dashed curves are the experimental data for $N_c = 0$ *(2),* $N_c^{at} = 0.61$ *(4),* $N_c^{at} = 0.22$ *(5),* $N_c^{at} = 0.18$ *(6),* $N_c^{at} = 0.16$ *(7), solid curves are theoretical calculations for free atmosphere (1) and under the conditions of thermal blooming (3).*

Burning aerosol particles may cause small–scale inhomogeneities of the refractive index. A duration of single generation pulse creating the HPLR channel satisfies the condition

$$\tau_p < \frac{a_1 + a_f}{2\, V_s}, \qquad (N^{1/3}\, V_s)^{-1} \le \tau_p \le (3\, N^{2/3}\, \chi)^{-1}, \qquad (9)$$

where $N = 10^3$ cm^{-3} is the aerosol particle number density; $V_s = 330$ m/s is the speed of sound.

According to Ref. 11 a stochastization of the medium in the channel because of the overlapping refracting halos from the absorbing centers randomly located in the space takes place under the above mentioned conditions. Size of thus induced perturbations are small as compared with the size of turbulent inhomogeneities. This leads to the second scale at a shorter correlation time.

In addition the high–frequency fluctuations of the refractive index may be caused by the acoustic waves generated under the action of pulse or pulse–periodic radiation and propagating through the HPLR channel. The change in the refractive index is related to the change in medium density as follows[12]

$$\Delta n \approx 3 \cdot 10^{-4}\, \Delta\rho \,/\, \rho_0, \qquad (10)$$

where ρ_0 is the equilibrium value of density.

In Ref. 13 it was shown that the maximum density change in the channel was observed during the time $t = a/V_s$. This time exceeds the pulse duration by an order of magnitude. After this time the density perturbations decrease and then, as a result of gas dynamics relaxation, the medium density reaches the equilibrium value determined at the beam axis by the value

$$\rho_0 \simeq \alpha_{ab}\, (\gamma - 1)\, V_s^{-2}\, E_0,$$

where γ is the adiabatic exponent; E_0 is the pulse energy density. Then the heat is removed from the channel due to

thermal conductivity and wind. Estimations made using the results from Ref. 13 for the equilibrium values of density change at the medium absorption coefficient $\alpha_{ab} \simeq 2 \cdot 10^{-6}$ cm^{-1} obtained experimentally give the value $\Delta\rho/\rho \simeq 0.7 \cdot 10^{-5} E_0$ that corresponds to $\Delta n \simeq 2 \cdot 10^{-6} E_0$. The changes in the refractive index can reach the values comparable with the atmospheric inhomogeneities at sufficiently high pulse energy density.

So, under the action of pulse–periodic radiation the refractive index in the channel changes periodically at a pulse repetition frequency.

Calculations carried out in Ref. 14 in the approximation of the short pulse $\tau_p << \tau_s = a/V_s$ when thermal blooming is absent showed that the presence of channel essentially changed the statistical pattern of the time fluctuations in the sounding beam intensity as compared with the propagation without the action of HPLR. In the channel the time correlation function becomes bimodal.

The first correlation scale (low–frequency) is related to the time of medium inhomogeneities travel across the sounding beam at a mean wind speed. The second scale being determined by the fall of $B_I(\tau)$ to the half level is connected with the time of sound wave run through the channel cross section τ_s. The higher is the channel optical strength, the more essential are the acoustic changes of density, and therefore the change of the level of sounding radiation correlation becomes higher. The curves *1* and *3* presented in Fig. 8 were calculated by formulas from Ref. 14 for the intensity fluctuations in the free atmosphere (curve *1*) and in the channel (curve *3*) with the parameters close to the experimental conditions. As is clear from Fig. 8, the calculated and experimental data are in a good agreement. This is indicative of the essential influence of the density perturbations on the parameters of sounding beams propagating through the channel.

8. Thus, the integrated analysis of the experimental studies of the HPLR propagation along the atmospheric path allows the following regularities in the influence of the atmospheric conditions on the HPLR parameters to be formulated:

– the atmospheric transfer ratio for a HPLR beam energy at the ground paths can be predicted based on the linear transmission calculated from the measured meteorological parameters under weak aerosol turbidity of the atmosphere;

– the energy density at the intensity maximum in the focusing plane depends on the generalized parameter of nonlinear distortions being determined by the propagation conditions at the path and HPLR parameters; the density decreases by a factor of 2–2.5 when this parameter increases from 0.3 to 2; an empirical dependence of the energy density at maximum on the parameter N_c has been established;

– the beam radius in the focusing plane is determined by the wind direction and speed if the speed $V_\perp > 1$ m/s. In this case during the time of the order of the time of medium travel across the beam, the beam radius increases by a factor of 1.5; under the longitudinal and weak transverse wind ($V_\perp < 0.5$ m/s) the beam radius increases by a factor of 2–2.5 during 0.4 s; in a stationary regime the beam broadening depends on the value of nonlinearity parameter in the initial segment and on fluctuations of the transverse component of wind velocity;

– the stagnation segment located between the source and optical system essentially affects the HPLR beam parameters, so that for inhomogeneous paths the nonlinear–distortions parameter ought to be determined accounting for contributions from each segments of the path;

– at propagation of pulse–periodic radiation in the HPLR channel the acoustic waves can occur leading to the high–frequency amplitude modulation of sounding radiation.

REFERENCES

1. V.E. Zuev, A.A. Zemlyanov, and Yu.D. Kopytin, *Nonlinear Optics of the Atmosphere* (Gidrometeoizdat, Leningrad, 1989), 255 pp.
2. V.V. Vorob'ev, *Thermal Blooming of Laser Radiation in the Atmosphere* (Nauka, Moscow, 1987), 200 pp.
3. D.K. Smitt, Proc. IEEE **65**, N0. 12, 59–103 (1987).
4. V.P. Lukin, *Atmospheric Adaptive Optics* (Nauka, Novosibirsk, 1986), 246 pp.
5. V.E. Zuev and M.V. Kabanov, *Transfer of the Optical Signals in the Earth's Atmosphere* (Sov. Radio, Moscow, 1977), 358 pp.
6. V.N. Aref'ev and V.I. Dianov–Klokov, Kvant. Elektron **3**, No. 4, 923–924 (1976).
7. V.A. Banakh, I.N. Smalikho, and A.V. Tailakov, Izv. Vyssh. Uchebn. Zaved. SSSR, Ser. Radiofiz. **31**, No. 11, 1409–1412 (1988).
8. V.V. Karasev, Yu.A. Konyaev, V.M. Sazanovich, et al., Atmos. Oceanic Opt. **6**, No. 4, 238–249 (1993).
9. B.M. Yavorskii and A.A. Detlaf, *Handbook on Physics* (Nauka, Moscow, 1971), 940 pp.
10. V.F. Baryshnikov, I.Ya. Shapiro, and A.P. Cherepanov, in: *Proceedings of X All–Union Symposium on the Laser Radiation Propagation through the Atmosphere*, Tomsk (1989), pp. 224–226.
11. V.V. Kolosov, *"Optical radiation propagation through the channels of clearing up due to aerosol explosion under exposure to laser radiation,"* Cand. Phys.–Math. Sci. Dissert., Institute of Atmospheric Optics, Tomsk (1982).
12. M. Born and E. Volf, *Principles of Optics* (Pergamon, New York, 1959).
13. V.V. Kolosov and A.V. Kuzikovskii, in: *Abstracts of Reports at II Meeting on Atmospheric Optics,* Tomsk (1982), pp. 67–69.
14. V.A. Banakh, V.L. Mironov, I.N. Smalikho, et al., Izv. Vyssh. Uchebn. Zaved. SSSR, Ser. Radiofiz. **30**, No. 5, 585–591 (1987).